eLIFE
elifesciences.org

Figures and figure supplements

Auditory synapses to song premotor neurons are gated off during vocalization in zebra finches

Kosuke Hamaguchi, et al.

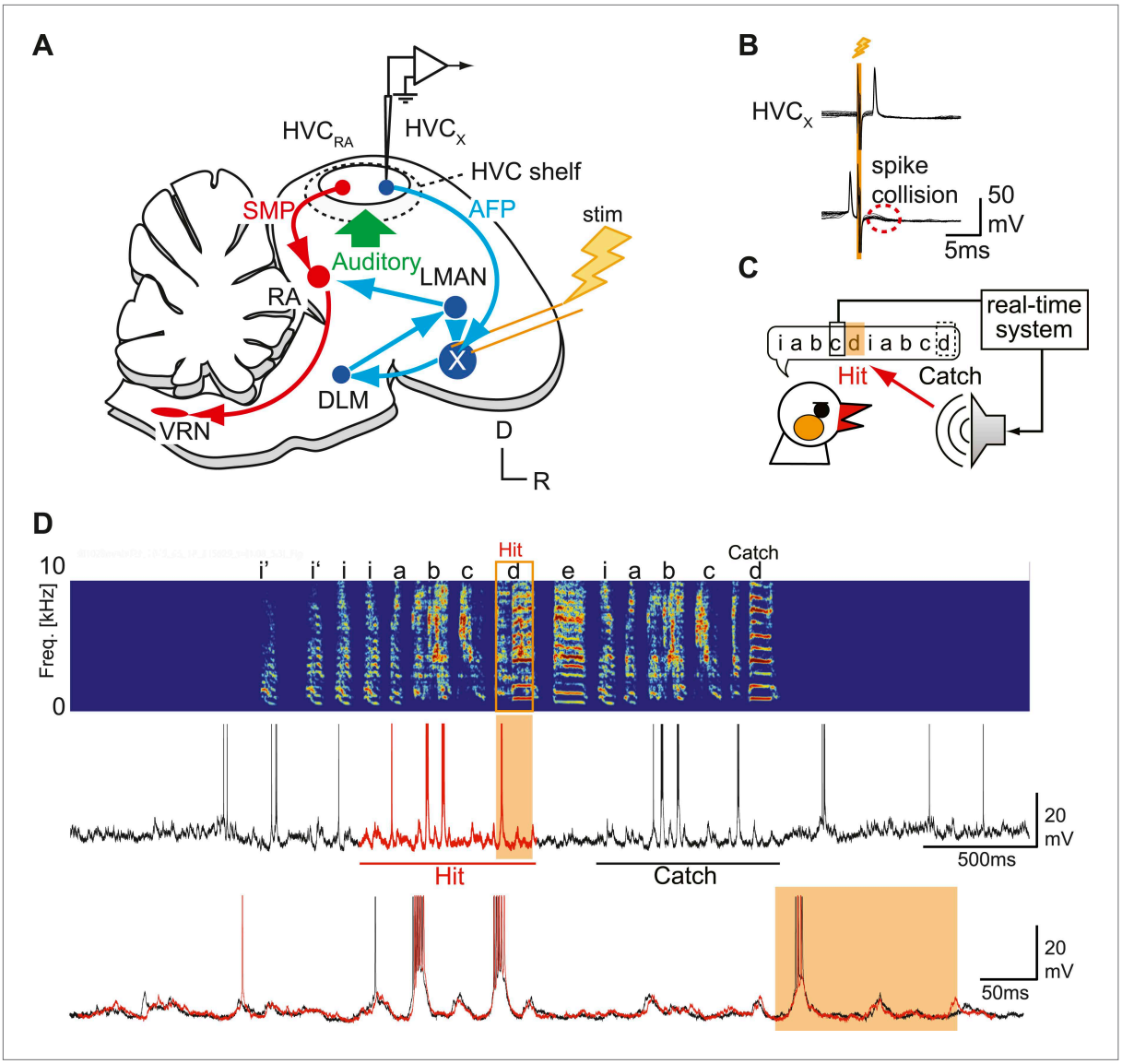

Figure 1. Sharp intracellular recordings from sensorimotor neurons in singing birds. (**A**) Schematic illustrates the configuration of the in vivo intracellular recording methods used to measure subthreshold activity of HVC_X neurons. Abbreviations: AFP, anterior forebrain pathway (light blue); SMP, song motor pathway (red); RA, robust nucleus of arcopallium; DLM, dorsolateral division of the medial thalamus; LMAN, lateral magno-cellular nucleus of the anterior nidopallium; VRN, brain stem vocal respiratory network, which includes the tracheosyringeal portion of the hypoglossal motor nucleus (nXIIts) and the respiratory premotor neurons located in the rostral ventrolateral medulla (RVL); R, rostral; D, dorsal. (**B**) Antidromic identification of HVC_X neurons was achieved by electrically stimulating Area X combined with spike collision tests. (**C**) The experimental design used to generate distorted auditory feedback (DAF). Shortly (~8 to 10 ms) after detecting that the bird sang the target syllable, a recorded version of the target syllable or a noise burst was played to the bird through a speaker (hit); DAF was suppressed on randomly chosen trials (catch). (**D**) Examples of HVC_X intracellular membrane potential recordings during hit and catch conditions. Top: sonogram. Middle: simultaneously recorded HVC_X neuron membrane potential. Bottom: expanded view of membrane potential traces aligned to the onset of the entire motif (iabcd), which was sung twice in this bout. The timing of DAF is shown in boxed and shaded regions.

DOI: 10.7554/eLife.01833.003

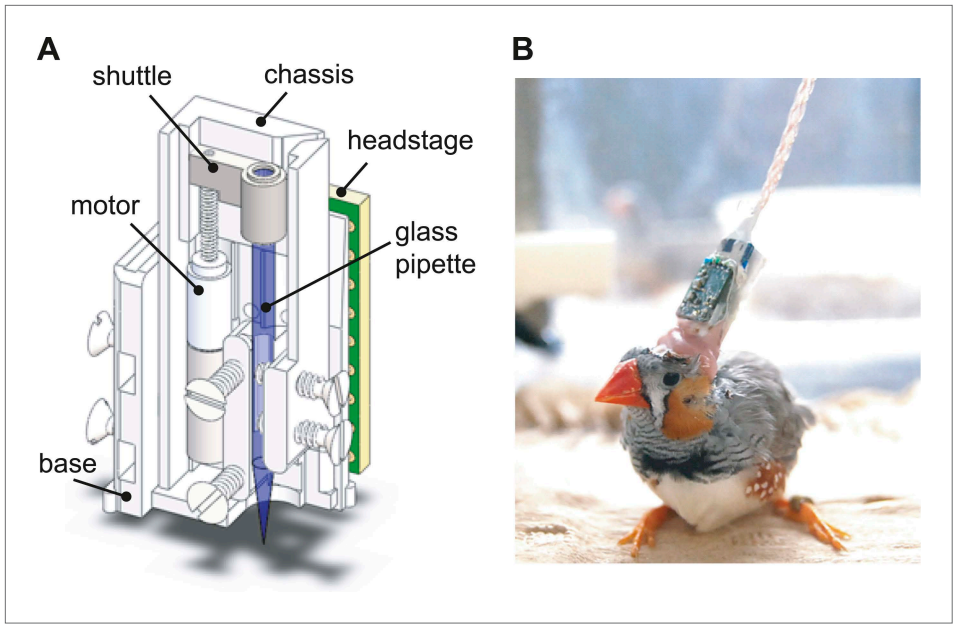

Figure 1—figure supplement 1. The design of the integrated intracellular microdrive used in these experiments.
DOI: 10.7554/eLife.01833.004

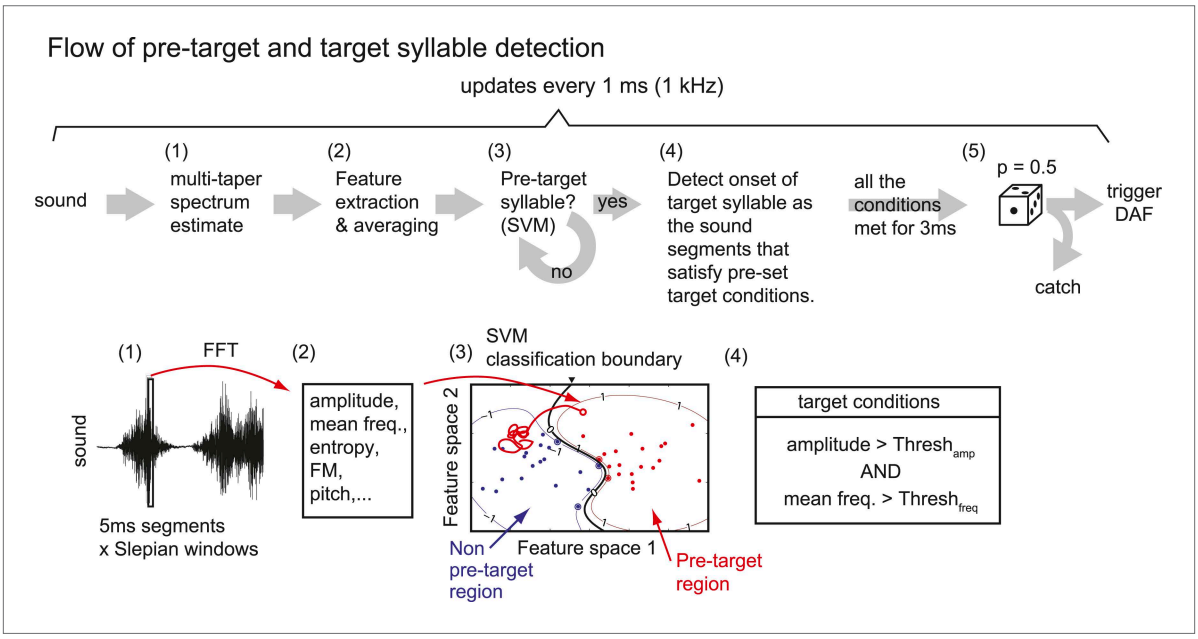

Figure 1—figure supplement 2. Flow of pre-target and target syllable detection.
DOI: 10.7554/eLife.01833.005

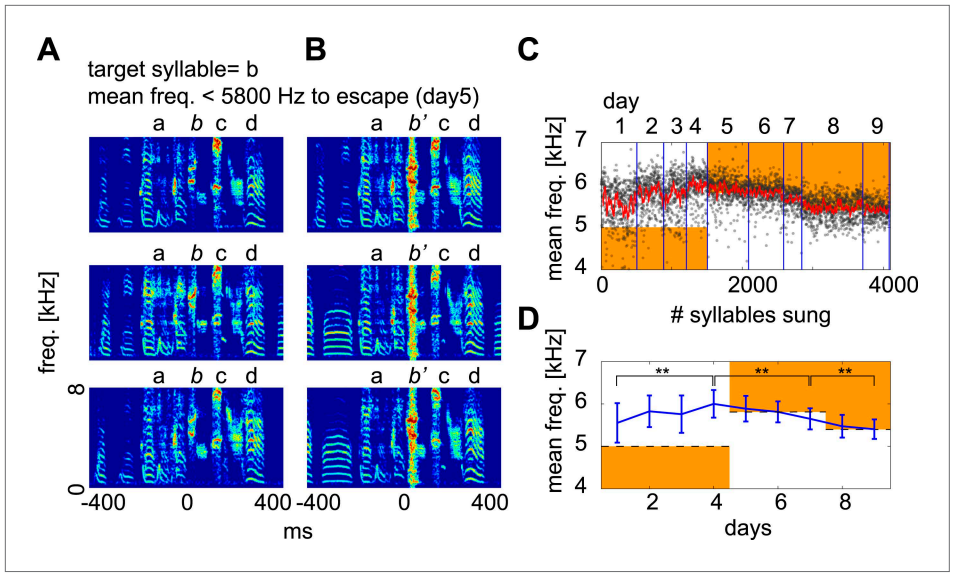

Figure 1—figure supplement 3. Contingent DAF drives adaptive changes in spectral features of the target syllable.

DOI: 10.7554/eLife.01833.006

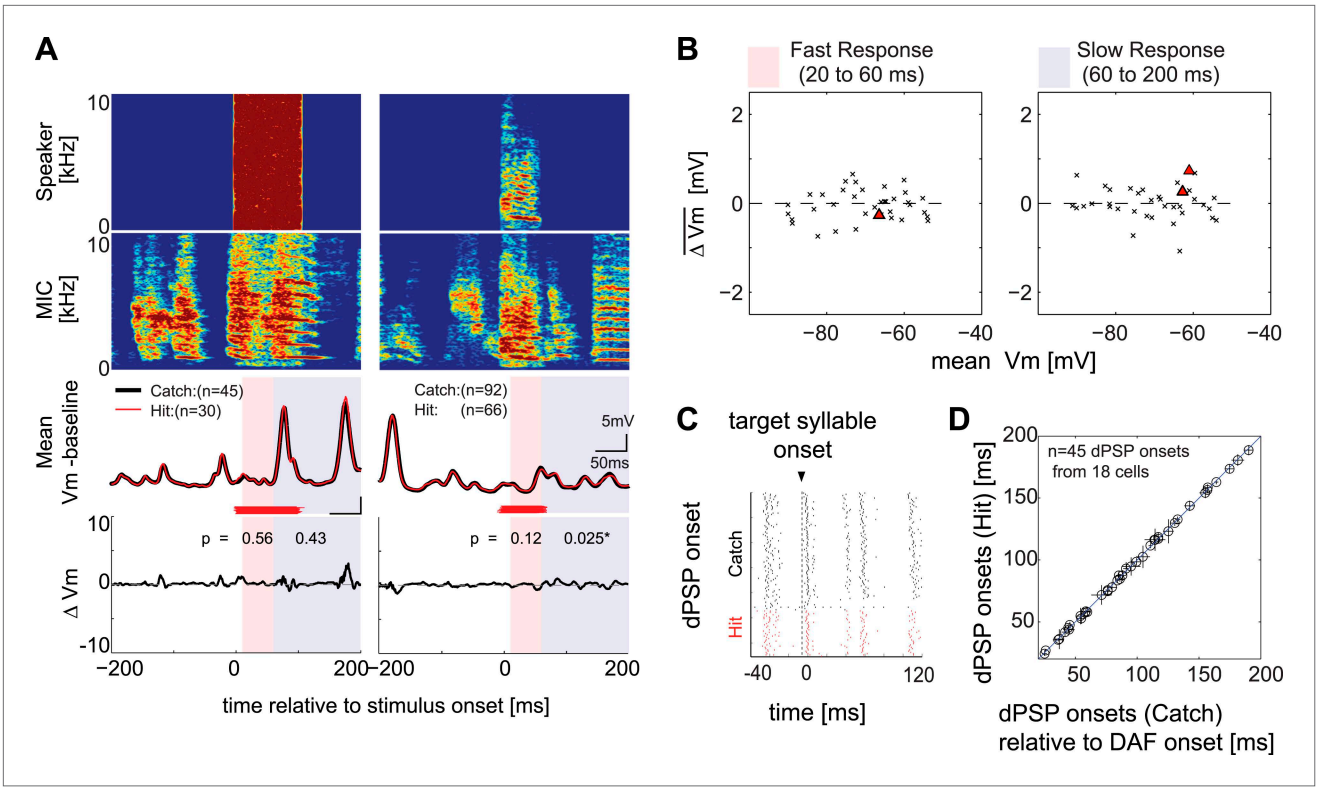

Figure 2. Synapses onto HVC_X neurons do not convey auditory feedback signals during singing. (**A**) Each row represents (from top to bottom) the speaker output (Speaker), microphone input (MIC), trial-averaged membrane potential activity in hit (red) and catch (black) trials relative to the baseline (defined as −200 to 0 ms before DAF onset), and the difference in membrane potential between hit and catch conditions (ΔV_m). Two examples of HVC_X singing-related subthreshold activity are shown. Two time ranges are set to bracket DAF onset and offset (fast: 20–60 ms, red-shaded region covers the fastest synaptic latency of HVC in response to auditory stimuli [***Lei and Mooney, 2010***]; slow: 60–200 ms, purple shaded region covers the remainder of the DAF period). Red horizontal lines indicate the timing of the DAF stimulus presented during each electrophysiological recording. Data are aligned to the onset of the target syllable, and time zero is set to the mean DAF onset. (**B**) Population analysis of time-averaged ΔV_m in fast and slow response windows showed no significant changes in response to DAF (n = 38 comparisons made from n = 34 cells; four cells were analyzed at both resting and at hyperpolarized membrane potentials. Individual cell-based analysis revealed that all except two cells showed non-significant changes; triangles [$p<0.05$], crosses [$p\geq0.05$, paired *t*-test]). (**C**) Examples of dPSP onset timings aligned to target syllable onset obtained from a single cell. (**D**) Onset timings of dPSPs measured in catch vs hit trials were indistinguishable (n = 45 dPSPs [1–4 dPSP onsets per cell] from 18 cells; see 'Materials and methods' for more information about dPSP onset detection and clustering methods used for peak detection; mean p=0.52, min p=0.06, *t*-test).

DOI: 10.7554/eLife.01833.007

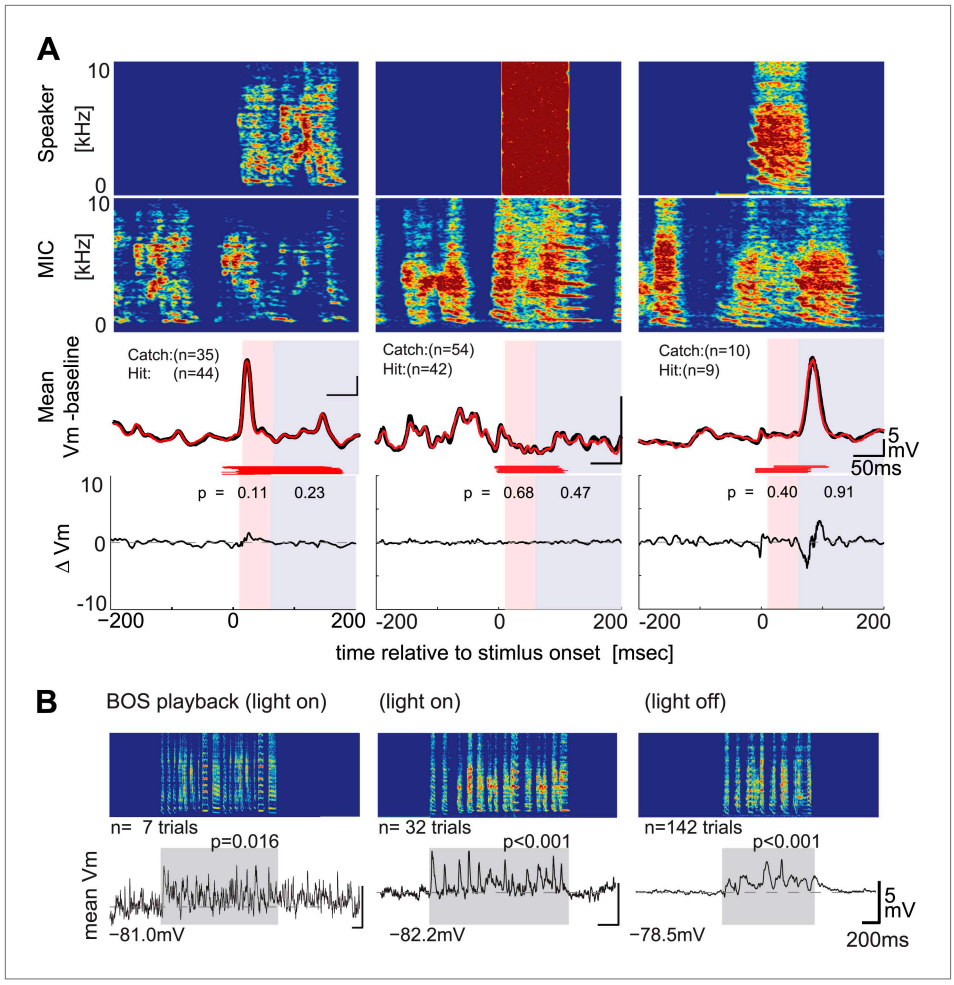

Figure 3. DAF-insensitive HVC_X cells can respond to auditory stimuli in non-singing states. (**A**) Examples of trial-averaged singing-related subthreshold activity of DAF-insensitive cells in hit and catch conditions, following the same scheme shown in ***Figure 2A***. (**B**) Examples of averaged subthreshold responses to BOS playback in the cells shown in (**A**) in day (light on) or night (light off) conditions. The significance of the BOS-evoked auditory response measured in non-singing states was determined either by the difference in the mean (Mann–Whitney *U*-test) or standard deviations (Ansari–Bradley test, a non-parametric test of variance) of the membrane potential fluctuations during the stimulus period and a pre-stimulus baseline period.

DOI: 10.7554/eLife.01833.008

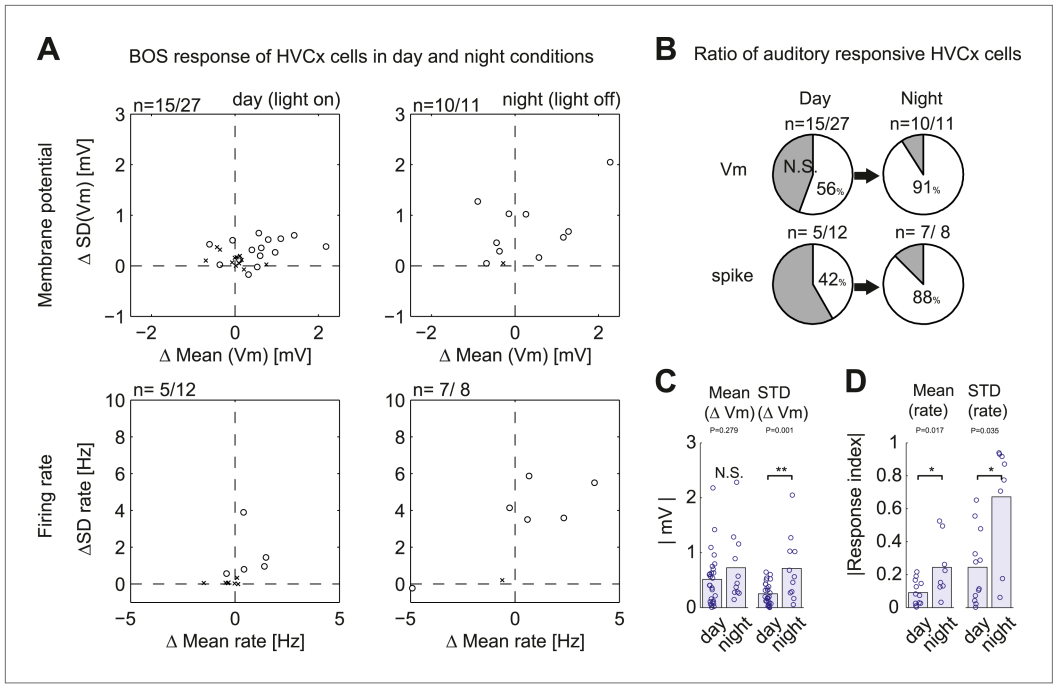

Figure 3—figure supplement 1. Summary of auditory responses of HVC_x cells in non-singing states.

DOI: 10.7554/eLife.01833.009

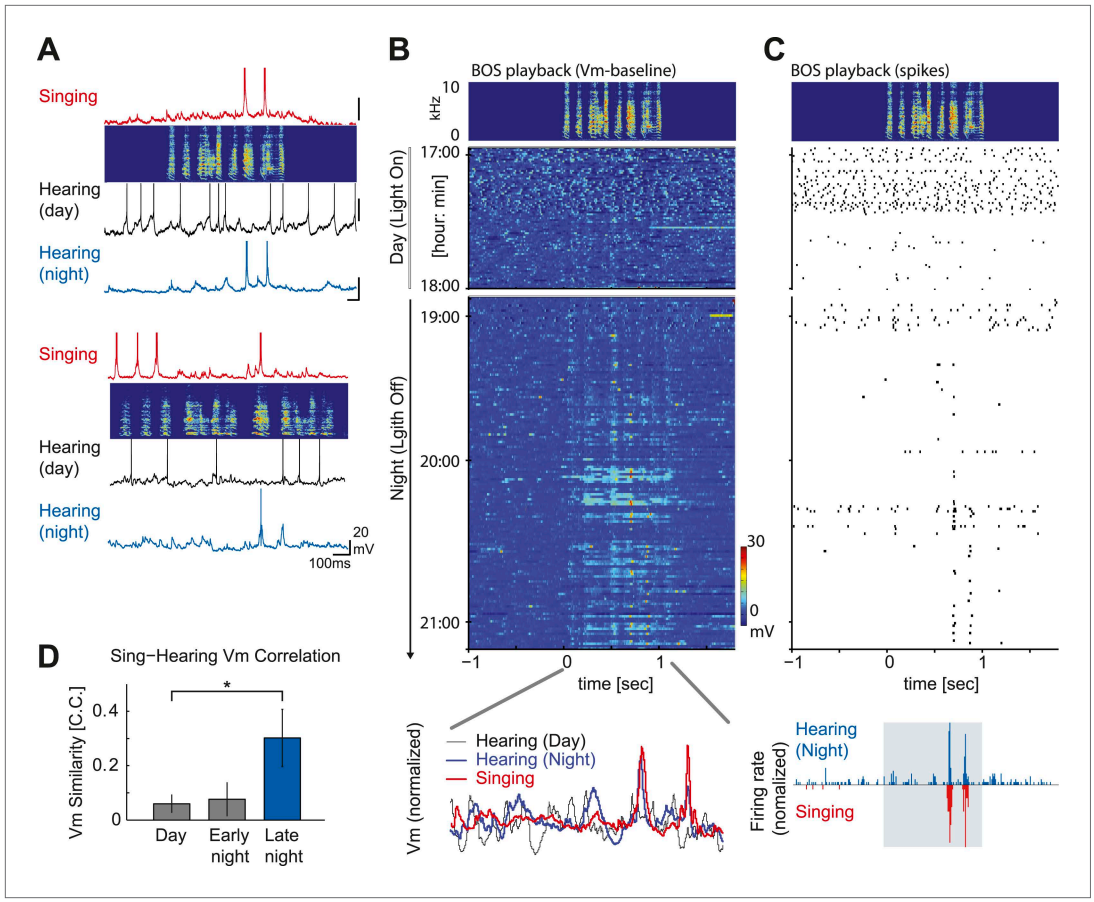

Figure 4. Auditory-vocal mirror neurons in zebra finches. (**A**) Examples of singing and auditory-related membrane potential activity of two HVC_X cells aligned to each bird's motif. Initially weak but significant auditory responses during the day (black) become robust during the night (blue) and precisely mirror the cell's singing-related activity (red). The cell at the top is the same cell shown in ***Figure 3*** (**A**) right, which lacked DAF sensitivity. (**B**) Emergence of robust BOS-evoked subthreshold activity as the night progresses. Top: BOS responses near the day–night boundary (same cell shown in ***Figure 4A***, top). Baseline-subtracted membrane potential responses aligned to the BOS playback (top panel) and shown in the order of the recording time. Bottom: normalized voltage trace of the cell's BOS evoked activity at day (black), night (blue) and singing-related activity (red). (**C**) The same cell's action potential response to BOS playback, plotted in the same scheme used in (**B**). 1–2 hr after nightfall, strong BOS-evoked action potential activity was detected that closely mirrored the singing-related activity recorded from this same cell 4–5 hr earlier, during the daytime. (**D**) Similarity of a cell's subthreshold activity during singing and hearing the same motif in the day or night measured by the correlation coefficient (C.C.) of averaged membrane potential records reveals enhanced similarity of singing-related and BOS-evoked activity later in the night (≥30 min after light off). Data are only from auditory-responsive cells in which we also collected singing data (singing vs hearing data during the day: n = 7, C.C. = 0.076 ± 0.041 (SEM); Early night, < 30 min after light off: n = 7, C.C. = 0.077 ± 0.061; Late night, ≥ 30 min after light off: n = 4, C.C. = 0.302 ± 0.105. Mann–Whitney *U*-test, p=0.04 compared to day).

DOI: 10.7554/eLife.01833.010

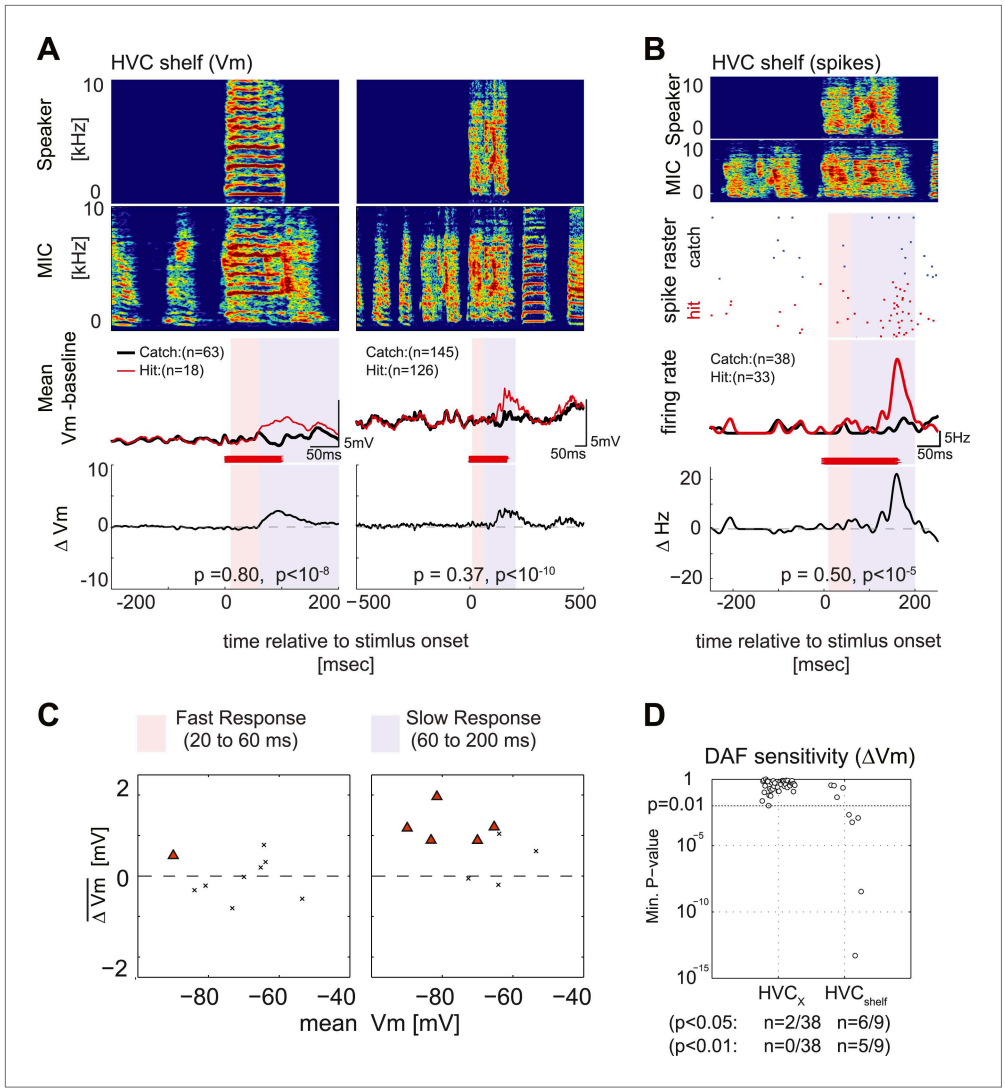

Figure 5. Synapses onto HVC shelf neurons convey DAF signals during singing. (**A**) Examples of trial-averaged subthreshold activity patterns of DAF-sensitive HVC shelf cells in hit and catch conditions, following the same scheme as ***Figure 2A***. Exposure to DAF significantly increased subthreshold depolarizations during singing. (**B**) An HVC shelf cell that showed a significant suprathreshold response to DAF, following the same scheme shown in ***Figure 2A*** except for the addition of a spike-rastergram in the second row. (**C**) Time-averaged ΔV_m in fast and slow response windows (n = 9 cells, triangles [p<0.05], crosses [p≥0.05, paired t-test]). (**D**) DAF sensitivity plot for HVC shelf neurons and HVC_X cells. Nearly half of the HVC shelf neurons showed DAF sensitivity. The minimum p-values of time-averaged ΔV_m either in fast or slow time window are plotted, Mann–Whitney *U*-test.

DOI: 10.7554/eLife.01833.011

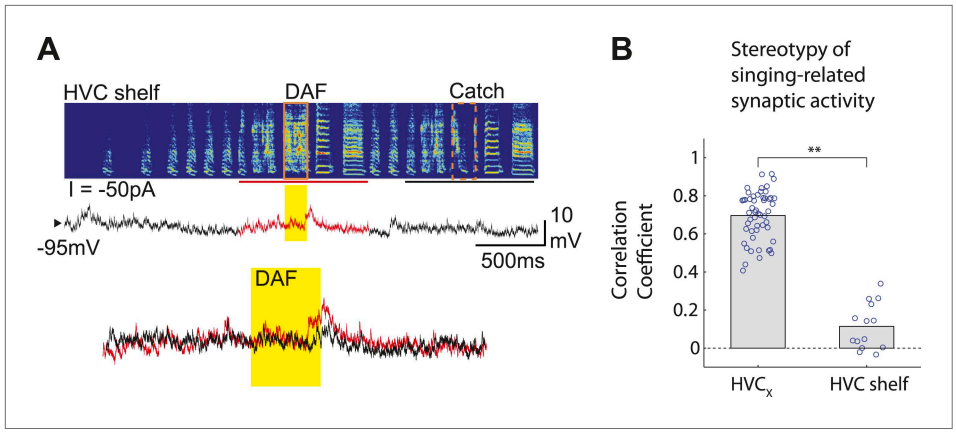

Figure 5—figure supplement 1. HVC shelf cells show subthreshold DAF sensitivity.

DOI: 10.7554/eLife.01833.012

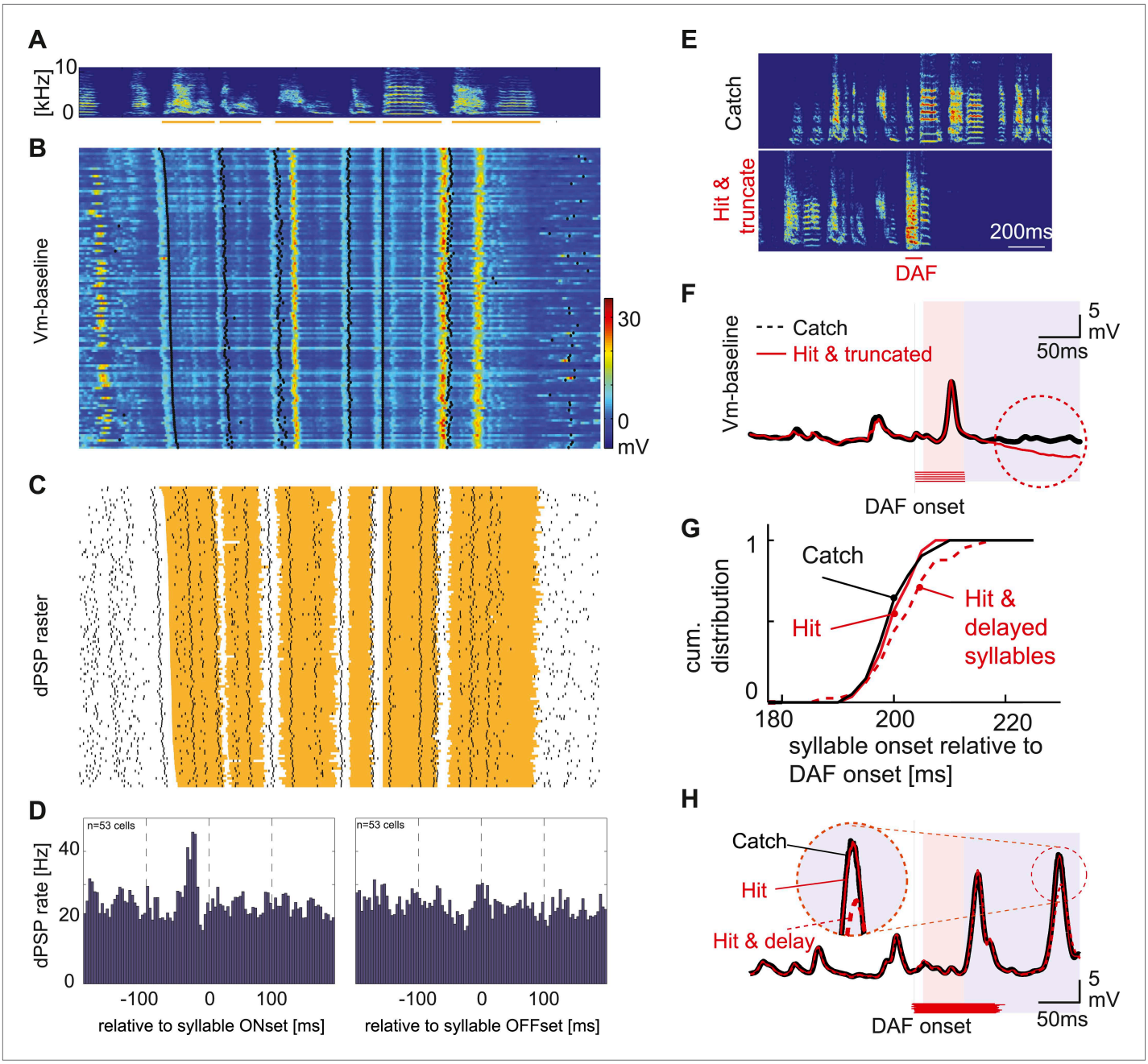

Figure 6. Synaptic inputs onto HVC_X cells encode future syllable onsets. (**A**) An example of a stereotyped syllable sequence, with syllables underlined by orange bars. (**B**) Pseudo-color representation of the membrane potential patterns relative to baseline while the bird sang many repetitions of the syllable sequence shown in (**A**). Black dots; syllable onsets. Data are aligned to a specific syllable and sorted from long to short motifs, which reflect natural variations in zebra finch song tempo. (**C**) Same data shown in (**B**), but dPSP onsets are shown by black dots, and the timing of individual syllables is represented by the orange regions. (**D**) Syllable onset- and offset-triggered average of dPSP onset rate (n = 53 HVC_X cells). (**E**) Example spectrograms from catch and 'hit-and-truncated' songs. (**F**) Trial-averaged subthreshold activity during hit-and-truncated songs showed a clear deviation from activity during catch trials. (**G**) Cumulative histogram of syllable onset timings relative to DAF onset in hit trials including delayed syllables (red dashed line), hit trials without delayed syllables (red solid line), and catch trials (black line). (**H**) Examples of trial-averaged subthreshold activity reveal that delayed motor output drives changes in the subthreshold activity (compare black and red dashed lines). After removing hit trials with delayed syllables, the subthreshold activity in hit and catch conditions is nearly identical (black vs red solid lines).

DOI: 10.7554/eLife.01833.013

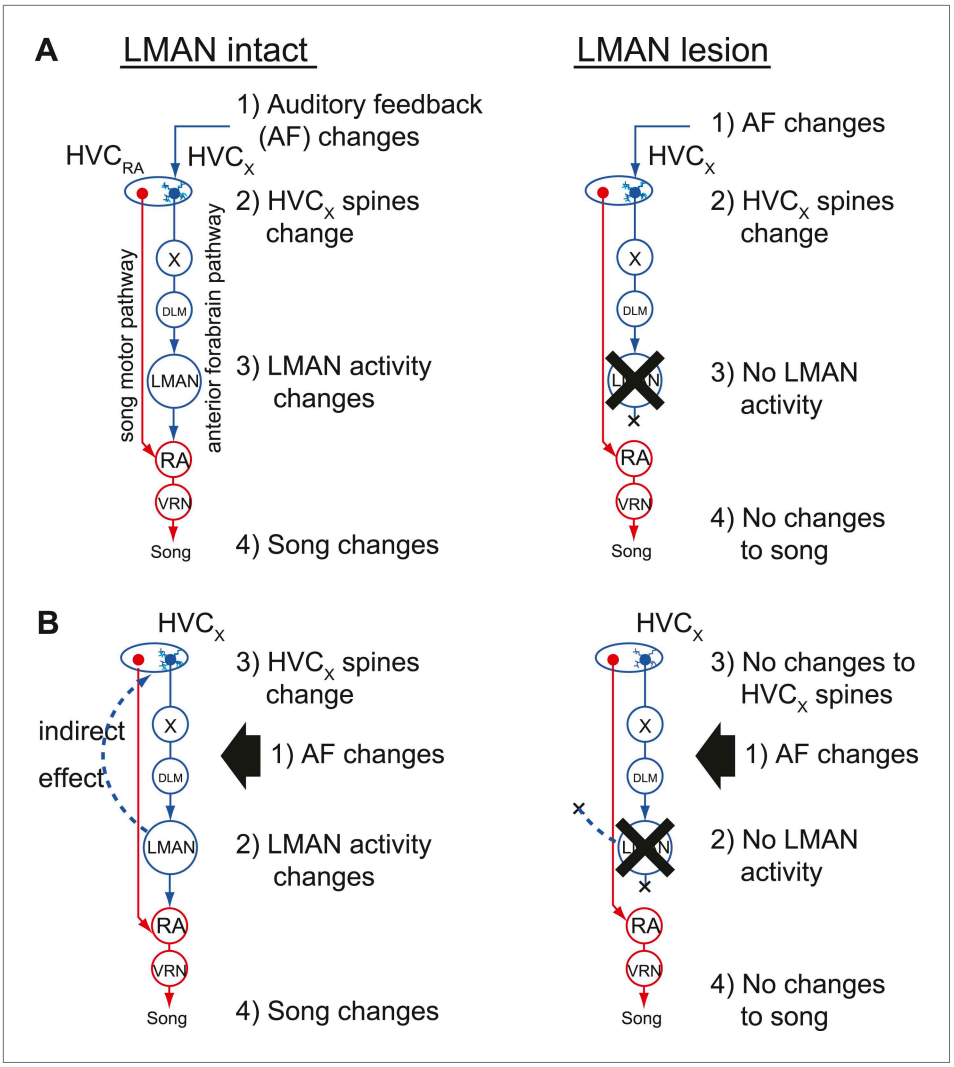

Figure 7. Two models of auditory feedback-dependent vocal and HVC dendritic plasticity. (**A**) A model where deafening triggers slow changes to HVC_X spines, subsequently altering AFP activity, which in turn drives vocal plasticity. In this model, LMAN lesions prevent deafening-induced song degradation but will not prevent deafening-induced changes to HVC_X spines. (**B**) A model where deafening acts through LMAN to trigger song plasticity and also to drive changes to HVC_X spines. In this model, LMAN lesions will prevent both deafening-induced song degradation and deafening-induced changes to HVC_X spines.

DOI: 10.7554/eLife.01833.014

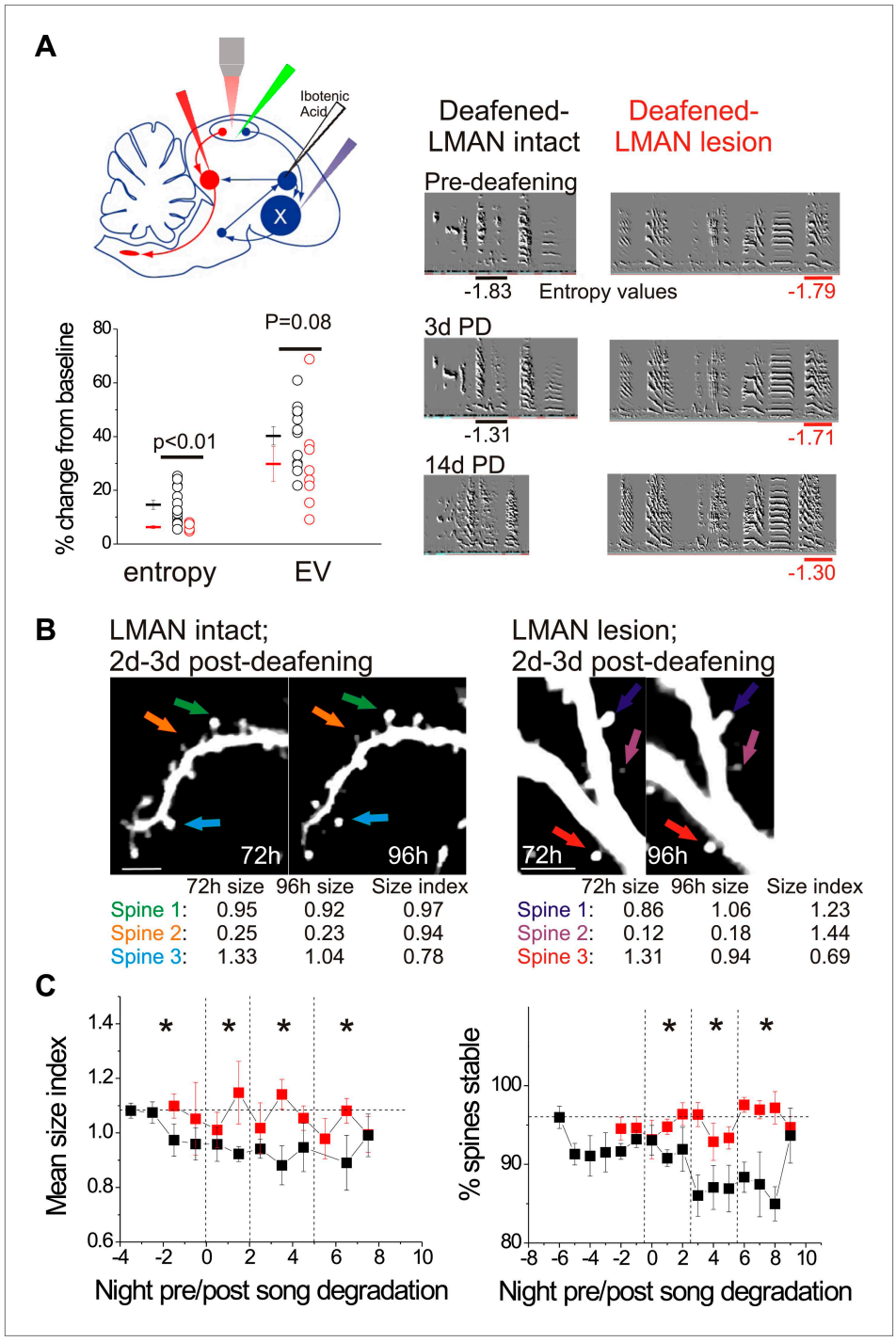

Figure 8. LMAN lesions prevent decreases in spine size and spine stability in HVC_X neurons following deafening. (**A**) Upper left: schematic illustrates surgical manipulations for in vivo imaging experiments. Lower left: quantification of deafening-induced changes to syllable entropy and EV at 3 days post-deafening in LMAN intact (black) and LMAN lesion (red) birds (only syllables that underwent significant degradation by 3 days post-deafening are shown; song degradation analyzed in a total of 6 LMAN lesion birds (3 used for imaging) and 19 LMAN intact birds (13 used for imaging in ***Tschida and Mooney, 2012***); entropy: 14 syllables from 10 LMAN intact birds, 5 syllables from 5 LMAN lesion birds; EV: 12 syllables from 9 LMAN intact birds, 8 syllables from 4 LMAN intact birds). Right: representative songs before and after deafening from LMAN lesion and LMAN intact birds. Deafened birds that received LMAN lesions still undergo subtle but significant song degradation. (**B**) Representative in vivo, two-photon images of HVC_X neurons showing changes in spine size between 2 and 3 days post-deafening in deafened birds with or

Figure 8. Continued on next page

Figure 8. Continued

without LMAN lesions (images of HVC_X dendrites from LMAN intact bird are reprinted with permission from ***Figure 1B*** in ***Tschida and Mooney, 2012***, Neuron, copyright Elsevier 2012, All Rights Reserved). LMAN lesions prevent the decrease in the size of HVC_X spines that normally follows deafening (size index <1 in LMAN intact birds). Scale bars, 5 μm. (**C**) Spine size index (left) and spine stability (right) is significantly higher in deafened birds with LMAN lesions. Quantification of spine size (left) and stability (right) in HVC_X neurons from deafened birds with (red) and without (black) LMAN lesions (LMAN intact data were previously reported in ***Tschida and Mooney (2012)***, except the values reported here have not been normalized to baseline, pre-deafening measurements). Time bins with significant differences between intact and LMAN lesion groups are indicated with asterisks ($p<0.05$).

DOI: 10.7554/eLife.01833.015

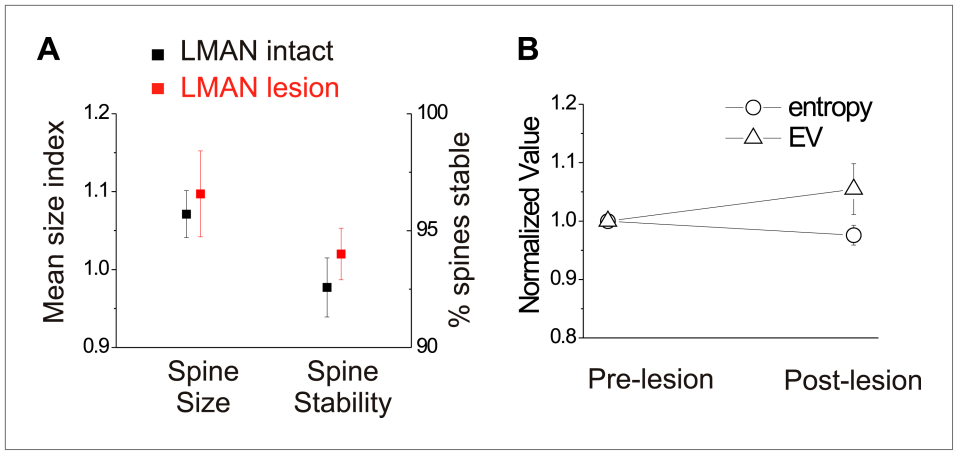

Figure 9. In birds with normal hearing, LMAN lesions do not significantly affect HVC_X spine dynamics or spectral features of song. (**A**) LMAN lesions affect neither spine size index nor spine stability in HVC_X neurons ($p=0.62$ for size, $p=0.61$ for stability; LMAN intact data were previously reported in ***Tschida and Mooney, 2012***). (**B**) LMAN lesions do not affect mean syllable entropy or EV (pre-lesion songs compared to songs from 4 to 5 days post-lesion; 25 syllables from 6 birds, $p=0.09$ for difference in mean entropy, $p=0.25$ for mean EV.

DOI: 10.7554/eLife.01833.016